Guided electromagnetic waves for damage detection and localization in metallic plates: numerical and experimental results

Jochen Moll [ORCID]

Goethe University of Frankfurt, Department of Physics, 60438 Frankfurt, Germany

Abstract

Electromagnetic waves in the microwave and millimeter-wave frequency range are used in non-destructive testing and structural health monitoring applications to detect material defects such as delaminations, cracks, or inclusions. This work presents a sensing concept based on guided electromagnetic waves (GEW), in which the waveguide forms a union with the structure to be inspected. Exploiting ultra-wideband signals a surface defect in the area under the waveguide can be detected and accurately localized. This paper presents numerical and experimental GEW results for a straight waveguide focusing on the detection of through holes and cracks with different orientation. It was found that the numerical model qualitatively replicates the experimental S-parameter measurements for holes of different diameters. A parametric numerical study indicates that the crack parameters such as its orientation and width has a significant influence on the interaction of the incident wave with the structural defect. On top, a numerical study is performed for complex-shaped rectangular waveguides including several waveguide bends. Besides a successful damage detection, the damage position can also be precisely determined with a maximum localization error of less than 3%.

Introduction

Electromagnetic waves at microwave and millimeter-wave frequencies have many interesting properties for non-destructive testing (NDT) of technical structures and components [1]. They are able to penetrate dielectric materials and provide information about the material's spectral response [2]. A structural defect, such as a delamination, can be measured based on a local change in the electromagnetic properties [3]. In contrast to related techniques the electromagnetic NDT methods are non-contact, enable a one-sided scanning, are free of couplants and without safety concerns due to the low radiated power [4]. Furthermore, surface defects in metallic structures can be detected by reflection coefficient-based methods using waveguide probes [5] and resonance frequency-based methods [6].

Recently, mm-waves were used in the context of structural health monitoring (SHM) for the detection [7] and localization [8] of structural defects in rotor blades of wind turbine structures. The same technology was used in [9] to monitor wind turbine blades in the field. Other examples where mm-waves were used for SHM purposes include mechanical vibration sensing exploiting the Doppler effect [10] or non-contact tip-clearance measurements of gas turbines [11]. In this work, guided electromagnetic waves (GEW) are considered that have recently been used for surface damage detection in metallic structures [12]. In addition, waveguide patches can be used for local hotspot monitoring [13, 14].

This paper presents numerical and experimental results for GEW propagation in a straight waveguide focusing on the detection of through holes and cracks with different orientation. For the first time, a numerical study is performed for complex-shaped rectangular waveguides including several waveguide bends. For this case, the damage position is determined and the accuracy of damage localization assessed.

The remainder of the paper is organized in the following way. Section "Methods" reports on the methods used in this work including a description of the simulation model, the measurement setup, and the damage localization approach. Section "Damage detection in straight waveguides" presents the numerical and experimental results for the case of a straight waveguide. After that, section "Detection of through holes in a complex-shaped waveguide" aims at damage analysis of a complex-shaped waveguide. Finally, conclusions are drawn at the end.

Methods

Detection concept

Figure 1 illustrates the underlying concept where the rectangular metallic waveguide forms a permanent union with the metallic host structure. A surface damage can be detected in the
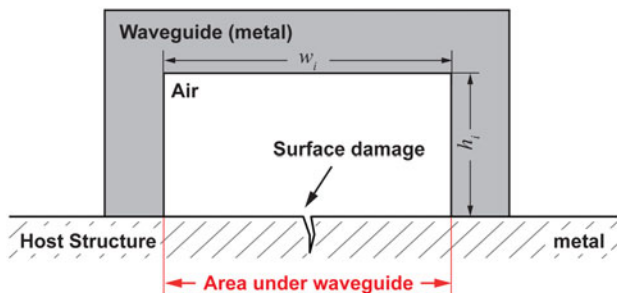
Fig. 1. Visualization of guided electromagnetic waves in a jointed electromagnetic waveguide. A rectangular waveguide is placed on top of a planar host structure where the inner faces form the wave guiding region. A surface damage can be detected in the area under the waveguide.

area under the waveguide by means of ultra-wideband signals in the frequency range from 20 to 40 GHz. Changes in the waveguide, e.g. due to abnormalities such as surface cracks, are detectable by microwaves–waveguide interactions from a single access point that is relatively far away. The signal processing for waveguides with a length of many tens of meters is straightforward, because only a single reflection and/or transmission measurement must be analyzed which is sufficient for sensitive damage detection and accurate damage localization. The proposed methodology benefits from recent developments in the field of additive manufacturing of passive high-frequency components [15, 16].

Numerical modeling

This paper considers two structures depicted in Fig. 2. The straight geometry is based on a standard rectangular waveguide WR 28 with a length of 400 mm. In this waveguide, the cutoff frequency of the lowest order mode is 21 GHz. The second structure has a complex geometry including several waveguide bends. The waveguide itself as well as the planar host structures are made of aluminum. The waveguide has an inner width of $w_i = 7.11$ mm and an inner height of $h_i = 3.55$ mm (see Fig. 1). In this research two practically relevant defect types are considered, namely through holes and cracks. The parameters of the damage types are also illustrated in Fig. 2. While the hole is characterized by its diameter D, the parameters of the rectangular crack are W_C, L_C, and θ. The axial position of the EM-wave in the waveguide is described by the x-coordinate. Numerical modeling has been performed in CST Microwave Studio using the time-domain solver.

Experimental measurements

The experimental setup shown in Fig. 3 is used to measure the straight waveguide. A network analyzer HP 8722C records the scattering parameters up to frequencies of 40 GHz in reflection and transmission mode. A flat aluminum sample (400 mm × 100 mm × 1 mm) represents the host structure. Drilling tools with diameters of 1–5 mm were used to create holes in the specimen of different sizes.

The network analyzer is calibrated prior to the measurements by means of an RF calibration kit. Due to the available calibration kit, the full bandwidth could not be exploited. The stimulus includes a low excitation amplitude of −15 dBm in the frequency range from 20 to 40 GHz. A total number of 201 frequency points
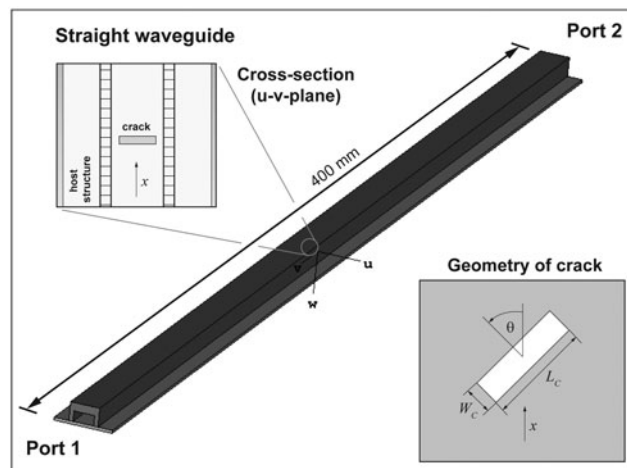
Fig. 2. (a) Straight waveguide with the geometry of the crack; (b) complex-shaped waveguide with three holes (hole #1, hole #2, hole #3) having a diameter of $D = 3$ mm.

were measured. The measurement data was downloaded to the PC for post-processing. More information on the signal-to-noise ratio (SNR) of the proposed setup can be found in [12].

Damage localization methodology

The damage localization approach is based on a differential S_{11} signal $s_d(t)$ between a baseline measurement from the intact structure $s_B(t)$ and the current measurement $s(t)$ that is measured from a structure with damage. The damage position x_D along the waveguide can be easily determined using the relationship

$$x_D = \frac{1}{2} t_0 c_{ph}(\omega_c) \tag{1}$$

In this equation, t_0 represents the time-of-flight of the scattered wave arriving at the input port. It can be determined from the signal $s_d(t)$, e.g. using threshold crossing. The frequency-dependent phase velocity is represented by $c_{ph}(\omega_c)$ where ω_c is the central frequency of the excitation pulse. Finally, the factor of 2 comes from the round trip path of the EM-wave from the input port to the damage and back.
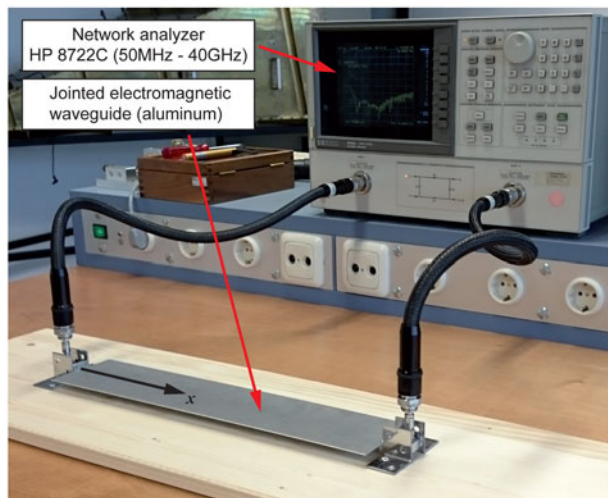
Fig. 3. Photo of the experimental setup showing the network analyzer HP 8722C (50 MHz–40 GHz) and the jointed electromagnetic waveguide. A flat aluminum sample (400 mm × 100 mm × 1 mm) represents the host structure in which holes were inserted.

Damage detection in straight waveguides

Detection of through holes

Figure 4 illustrates GEW propagation in a straight jointed rectangular waveguide for the intact and the damaged structure. While the incident wave, shown in Fig. 4(a), is the same in both cases, significant differences can be observed by comparing the wavefield from the undamaged and the damaged structure shown in Fig. 4 (b) and 4(c), respectively. The incident wave is reflected at the crack ($L_C = 5$ mm, $W_C = 1.5$ mm, $\theta = 90°$, $x = 200$ mm) and can be detected at the input port of the waveguide. Those reflections can be processed to assess the structural conditions.

Figure 5(a) shows the measured scattering parameters S_{11} where the undamaged structure is compared with the damaged structure for different hole sizes located at $x = 200$ mm. It can be observed that the S_{11} parameter increases as soon as the hole diameter becomes larger. This overall behavior can be modeled as shown in Fig. 5(b). A continuous increase of S_{11} over a wide frequency band can be observed for increasing hole sizes. However, due to the limited SNR in the experimental setup and the imperfections of the fabricated waveguide, the gap in S_{11} between the undamaged and the damaged waveguide is smaller in the experimental measurements compared to the numerical model.

Detection of cracks

The following section presents numerical results of a parametric study, where the crack parameters were systematically modified. The first result is depicted in Fig. 6 showing the scattering parameters S_{11} for different crack angles ranging from $\theta = 0°$ to $\theta = 90°$. In this example, the crack is located at $x = 200$ mm. First, it can be observed that the crack can be clearly distinguished from the baseline data, i.e. S_{11} measurements of the undamaged structure. Second, S_{11} increases steadily when the crack angle θ becomes larger. This result means that a crack oriented perpendicular to the direction of wave propagation can be detected easily compared to a coaxially aligned crack.

Next, Fig. 7 shows the identical crack parameters at different axial positions in the waveguide ranging from $x = 50$ mm to $x = 200$ mm.
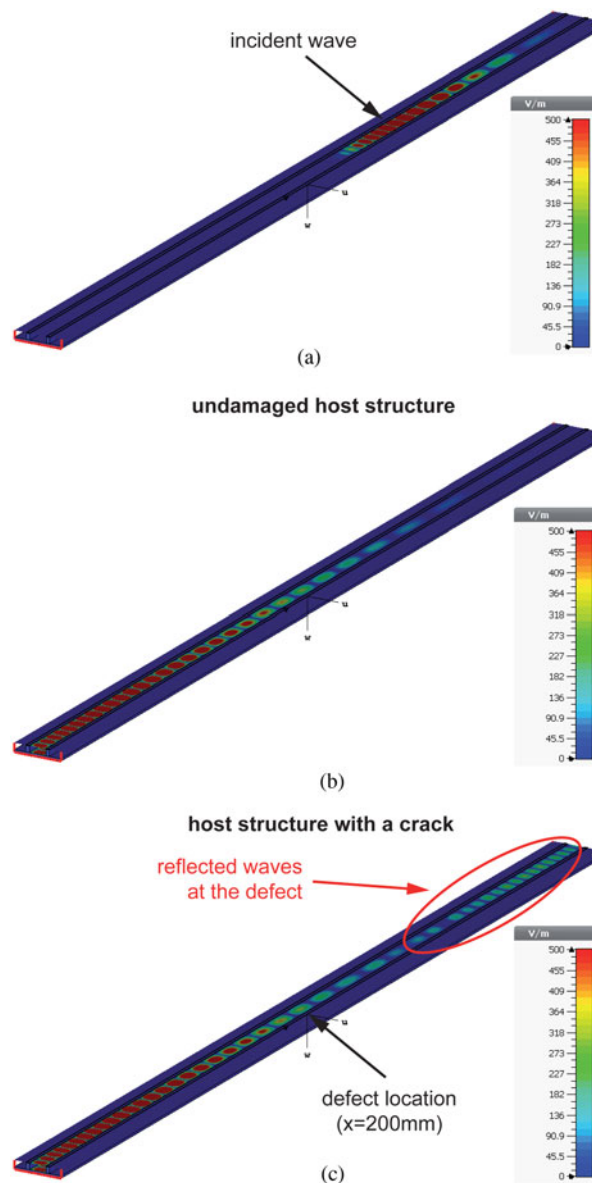

Fig. 4. Screenshots of wave propagation (electric field) in the straight waveguide as cross-sectional representation computed by CST Microwave Studio after (a) 0.8 ns and (b,c) 1.8 ns. In this example, the crack parameters are: $L_C = 5$ mm, $W_C = 1.5$ mm, $\theta = 90°$, $x = 200$ mm. Reflections at the defect can be observed by comparing the wavefield of the undamaged and the damaged structure.

It can be observed that unique features are preserved in the S_{11} parameters independent of the crack location in the waveguide. In any case, the crack can be clearly detected at all damage positions.

Finally, numerical results are presented in Fig. 8 showing a crack of 5 mm length and different widths positioned at $x = 200$ mm. From this plot it can be derived that the larger the crack width the easier it is to detect the damage by analyzing the S_{11} signals.

## Detection of through holes in a complex-shaped waveguide

The complex-shaped waveguide was placed in the numerical model on a 280 mm × 280 mm × 1 mm aluminum plate. Three damage scenarios in the form of through holes with a diameter of 3 mm have been modeled with their coordinates listed in
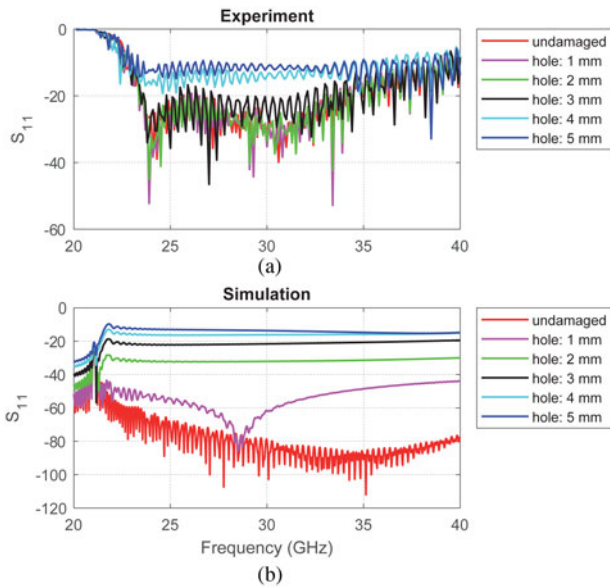
Fig. 5. Comparison between the experimental S_{11} measurements, after [12], and the numerical S_{11} predictions for the case of a through hole at $x = 200$ mm for various hole diameters. The numerical model is able to describe the experimental observations qualitatively.
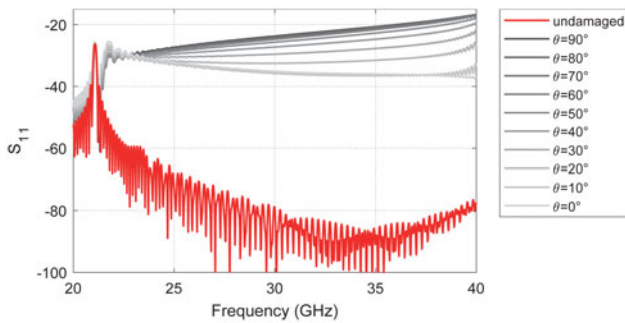

Fig. 6. Analysis of crack orientation at $x = 200$ mm ($L_C = 5$ mm and $W_C = 1.5$ mm). The orientation of the crack relative to the direction of wave propagation has a significant effect on the S_{11} parameters and hence the detectability of the crack. Coaxial orientation ($\theta = 0°$) leads to smaller S_{11} changes compared to an orthogonally aligned crack ($\theta = 90°$).
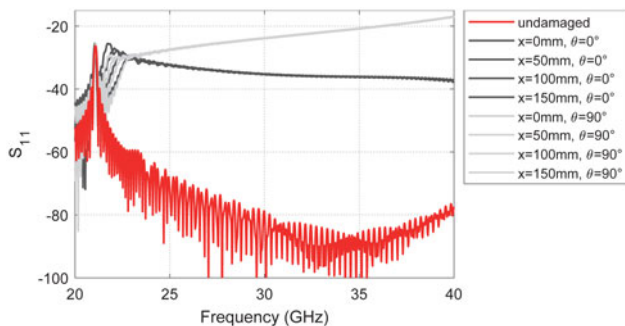
Fig. 7. Analysis of crack orientation at different axial positions in the waveguide. The position of the crack in the waveguide does not have a significant influence on the S_{11} characteristics, especially at frequencies larger than 23 GHz.

Table 1. The same excitation as before was used covering a frequency range from 20 to 40 GHz.

Figure 9 shows the S_{11} curves for all three damage cases. While the undamaged structure has a relatively low reflection over the
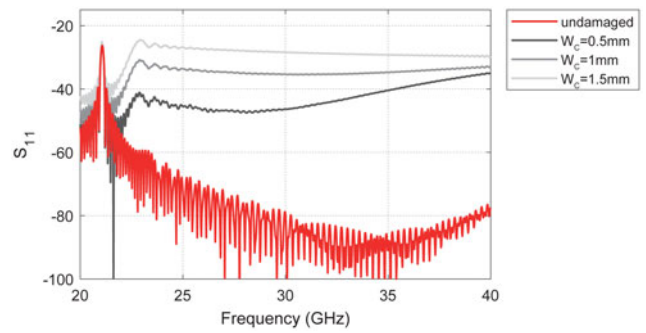
Fig. 8. Analysis of the detectability of a 5 mm long crack with different width at $x = 200$ mm. The larger the crack width the easier it is to detect it by the analysis of S_{11} measurements.

**Table 1.** Damage locations in the u–v-coordinate system of Fig. 2(b).

Description	u-position	v-position
Hole #1	−0.2254 m	0.1179 m
Hole #2	−0.1 m	0.055 m
Hole #3	−0.125 m	0.1808 m
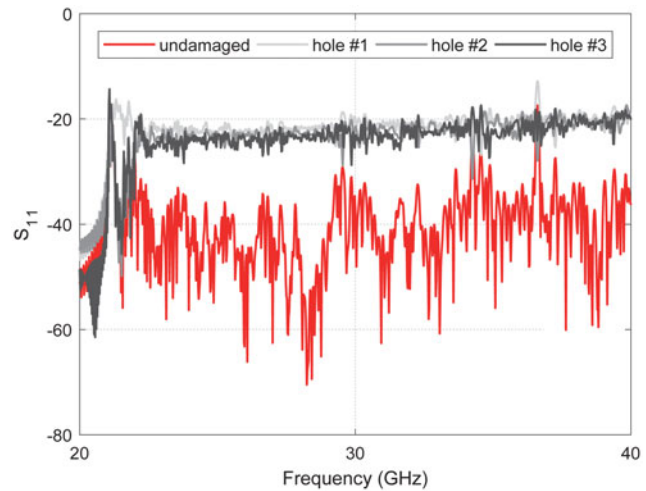
Fig. 9. Detection of holes at different locations in the complex-shaped rectangular waveguide. Each hole can be clearly identified based on an increase of S_{11}.

whole frequency band of interest, the S_{11} parameters increase for all three holes independent of their respective location in the waveguide. The result confirms that damage can be detected in a complex-shaped waveguide.

For practical applications it is of great interest to determine the damage location in order to optimize maintenance activities. Therefore, we have processed the time-domain S_{11}-signals for the undamaged and the damaged structure. The difference signals for all three cases are depicted with its spectrogram in Fig. 10. It can be observed that the time-of-flight t_0 for the three differential signals vary due to their respective location in the waveguide. Moreover, the wave propagation is dispersive so that the frequency-dependent wave velocity must be taken into account for transforming the time-domain signals into the distance domain. Here, we have used the center frequency of 30 GHz
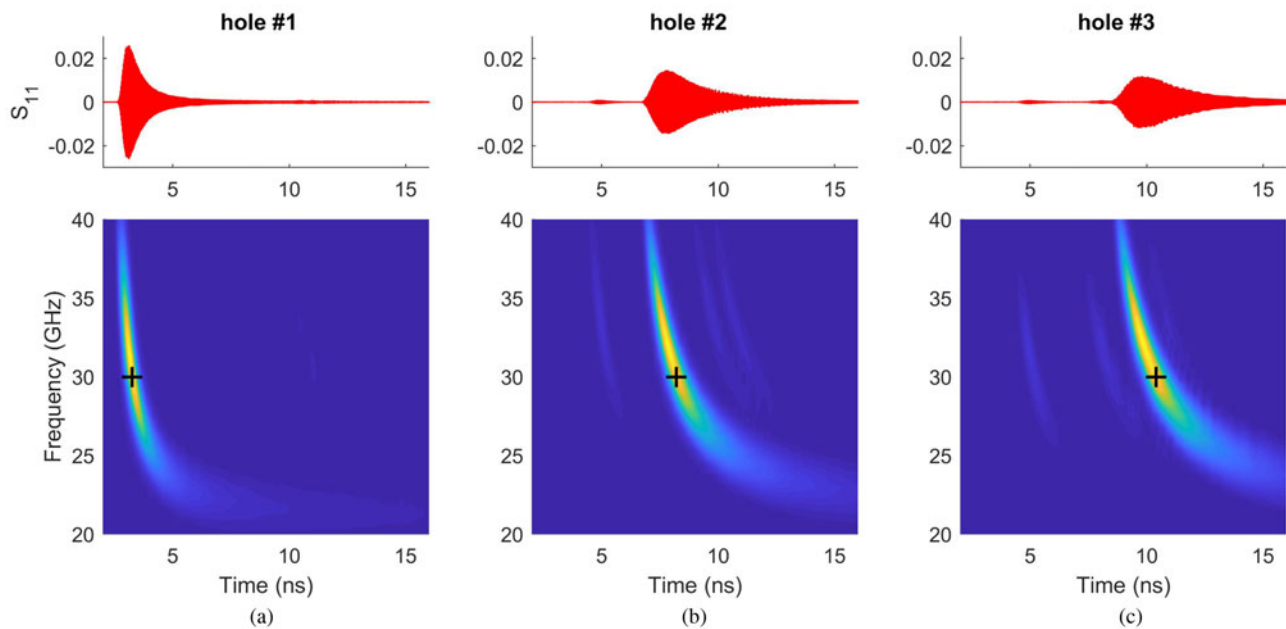
Fig. 10. (top) Time-domain analysis of the differential S_{11}-signal for (a) hole #1, (b) hole #2 and (c) hole #3; (bottom) spectrogram of the differential signals indicating the time delay at the mid frequency of 30 GHz.

Table 2. Accuracy of damage localization in the complex-shaped rectangular waveguides using reflection signals (relative to the total round-trip distance of 2.4884 m).

Description	Distance	Distance (estimated)	Error (%)
Hole #1	0.654 m	0.662 m	0.33%
Hole #2	1.719 m	1.672 m	1.88%
Hole #3	2.179 m	2.123 m	2.23%

which has a wave velocity of $2.04 \cdot 10^8$ m/s. Based on this value we have determined the axial position of the damage in the rectangular waveguide. The results are summarized in Table 2 showing that the localization error is always below 3%.

Conclusions

The research presented in this paper focused on the analysis of GEW propagation in a jointed electromagnetic waveguide. It was found that typical structural defects such as through holes and cracks can be successfully detected. A numerical model implemented in CST Microwave Studio is able to qualitatively describe the experimental S_{11} measurements in the frequency band from 20 to 40 GHz for the case of through holes with different diameters. Moreover, the numerical model predicts the scattering response of the incident electromagnetic wave at the crack. The main findings of the numerical study are summarized as follows:

- A crack oriented perpendicular to the direction of wave propagation can be detected easily than a coaxially aligned crack with the same dimensions.
- The S_{11} parameter does not change much when the crack is located at different positions in the waveguide.
- The larger the crack width, the easier it is to detect it.

- Damage can also be detected and precisely localized in a complex-shaped rectangular waveguide with multiple waveguide bends.

References

1. **Kharkovsky S and Zoughi R** (2007) Microwave and millimeter wave non-destructive testing and evaluation – overview and recent advances. *IEEE Instrumentation & Measurement Magazine* **10**(2), 26–38.
2. **Fukasawa R** (2015) Terahertz imaging: widespread industrial application in non-destructive inspection and chemical analysis. *IEEE Transactions on Terahertz Science and Technology* **5**(6), 1121–1127.
3. **Yang R, He Y and Zhang H** (2016) Progress and trends in nondestructive testing and evaluation for wind turbine composite blade. *Renewable and Sustainable Energy Reviews* **60**, 1225–1250.
4. **Li Z, Haigh A, Soutis C, Gibson A and Sloan R** (2017) Microwaves sensor for wind turbine blade inspection. *Applied Composite Materials* **24**(2), 495–512.
5. **Ali A, Hu B and Ramahi O** (2015) Intelligent detection of cracks in metallic surfaces using a waveguide sensor loaded with metamaterial elements. *Sensors* **15**(5), 11402–11416.
6. **Albishi AM and Ramahi OM** (2017) Microwaves-based high sensitivity sensors for crack detection in metallic materials. *IEEE Transactions on Microwave Theory and Techniques* **65**(5), 1864–1872.
7. **Moll J, Arnold P, Mälzer M, Krozer V, Pozdniakov D, Salman R, Rediske S, Scholz M, Friedmann H and Nuber A** (2018) Radar-based structural health monitoring of wind turbine blades: the case of damage detection. *Structural Health Monitoring* **17**(4), 815–822.
8. **Arnold P, Moll J, Mälzer M, Krozer V, Pozdniakov D, Salman R, Rediske S, Scholz M, Friedmann H and Nuber A** (2018) Radar-based structural health monitoring of wind turbine blades: the case of damage localization. *Wind Energy* **21**(8), 676–680.

9. **Moll J, Simon J, Mälzer M, Krozer V, Pozdniakov D, Salman R, Dürr M, Feulner M, Nuber A and Friedmann H** (2018) Radar imaging system for in-service wind turbine blades inspections: initial results from a field installation at a 2MW wind turbine. *Progress in Electromagnetic Research (PIER)* **162**, 51–60.

10. **Li C, Peng Z, Huang T-Y, Fan T, Wang F-K, Horng T-S, Munoz-Ferreras J-M, Gomez-Garcia R, Ran L and Lin J** (2017) A review on recent progress of portable short-range noncontact microwave radar systems. *IEEE Transactions on Microwave Theory and Techniques*, 1–15.

11. **Szczepanik R, Przysowa R, Spychaa J, Rokicki E, Kazmierczak K and Majewski P** (2012) Application of blade-tip sensors to blade-vibration monitoring in gas turbines. *In* Rasul M (ed). Thames Street London, UK: Headquarters IntechOpen Limited, pp. 145–176

12. **Moll J** (2018) Damage detection and localization in metallic structures based on jointed electromagnetic waveguides: a proof-of-principle study. *Journal of Nondestructive Evaluation* **37**(4).

13. **Moll J, Nguyen D and Krozer V** (2020) A numerical study on tomographic imaging using guided electromagnetic waves. *14th European Conference on Antennas and Propagation (EuCAP 2020)* (accepted in December 2019).

14. **Moll J** (2019) Numerical analysis of two-dimensional waveguide patches for surface damage detection. *12th German Microwave Conference*, IEEE, pp. 146–149.

15. **Zhang B, Chen W, Wu Y, Ding K and Li R** (2017) Review of 3D printed millimeter-wave and terahertz passive devices. *International Journal of Antennas and Propagation* **2017**, 1–10.

16. **Otter WJ and Lucyszyn S** (2017) Hybrid 3D-printing technology for tunable thz applications. *Proceedings of the IEEE* **105**(4), 756–767.

Jochen Moll received the Dipl.Ing. and Ph.D. degrees in mechanical engineering from the University of Siegen, Germany, in 2007 and 2011, respectively. Presently, he is a Postdoctoral Research Assistant with Goethe University Frankfurt, Germany. His research interests include non-destructive testing, structural health monitoring, and signal processing techniques. His research profile is located in

http://www.jochenmoll.de.